

Firing proprieties of an adaptive analog VLSI neuron

Daniel Ben-Dayan Rubin^{1,2}, Elisabetta Chicca², and Giacomo Indiveri²

¹ Department of Bioengineering, Politecnico di Milano,
P.zza Leonardo da Vinci 32, I-20133 Milan, Italy

² INI - Institute of Neuroinformatics - UNI/ETH Zurich,
Winterthurerstr. 190, CH-8057 Zurich, Switzerland
{dbd, chicca, giacomo}@ini.phys.ethz.ch

Abstract. We describe the response properties of a compact, low power, analog circuit that implements a model of a leaky I&F neuron, with spike-frequency adaptation, refractory period and voltage threshold modulation properties. We investigate the statistics of the circuit's output response by modulating its operating parameters, like refractory period and adaptation level and by changing the statistics of the input current. The results show a clear match with theoretical and neurophysiological data in a given range of the parameter space. This analysis defines the chip's parameter working range and predicts its behavior in case of integration into large massively parallel VLSI networks.

1 Introduction

Models of spiking neurons have complex dynamics that require intensive computational resources and long simulation times. This is especially true for conductance-based models that describe in details the electrical dynamics of biological neurons [1]. These models include non-linear voltage-dependent membrane currents and are difficult to analyze analytically and to implement. For this reason, phenomenological spiking neuron models are more popular for studies of large network dynamics. In these models the spikes are stereotyped events generated whenever the membrane voltage reaches a threshold. The Integrate-and-Fire (I&F) model neuron, despite its simplicity, captures many of the broad features shared by biological neurons. This model can be easily implemented using analog VLSI technology and can be used to build low power, massively parallel, large recurrent networks, providing a promising tool for the study of neural network dynamics [2, 3].

VLSI I&F neurons integrate presynaptic input currents and generate a voltage pulse when the integrated voltage reaches a threshold. A very simple circuit implementation of this model, the "Axon-Hillock" circuit, has been proposed by Mead [4]. In this circuit an integrating capacitor is connected to two inverters and a feedback capacitor. A pulse is generated when the integrated voltage crosses the switching threshold of the first inverter. An alternative circuit, proposed in [5], exhibits more realistic behaviors, as implements spike-frequency adaptation and has an externally set threshold voltage for the spike emission. Both circuits however have a large power consumption due to the fact that the input to the first inverter (the integrated voltage on the capacitor) changes slowly, typically with time constants of the order of milliseconds, and the inverter spends a large amount of time in the region in which both transistors conduct

a short-circuit current. The power consumption is reduced, but not optimized, in the circuit described in [6], using an amplifier at the input, to compare the voltage on the capacitor with a desired spiking threshold voltage. As the input exceeds the spiking threshold, the amplifier drives the inverter, making it switch very rapidly. In [7] Boahen demonstrates how it is possible to implement spike-frequency adaptation by connecting a four transistor “current-mirror integrator” in negative-feedback mode to any I&F circuit. An I&F circuit optimized with respect to power consumption but lacking of spike-frequency adaptation mechanisms, voltage threshold modulation, refractory period and explicit leak current is described in [8]. We designed a compact leaky I&F circuit, similar to previously proposed ones, that additionally is low power *and* has spike-frequency adaptation, refractory period and voltage threshold modulation properties [9]. In this work we characterize the circuit and compare its response properties to the ones predicted by theory and observed in neocortical pyramidal cells.

A typical feature exhibited by the majority of the pyramidal cells in neocortex and hippocampus, is the spike-frequency adaptation that depends on a Ca^{2+} -gated K^+ conductance. One of the aims of this study is the quantitative analysis of the performance of a circuit that reproduces this behavior. It has been shown that *in vitro* neocortical neurons exhibit *in vivo*-like activity when noisy inputs are injected [10, 11]. Inspired by these findings we measured the response function of the circuit to noisy input signals, by varying both circuit parameters and the parameters that control the statistics of the input current. The results described in this paper present a description of the integrated-circuit’s data in neurophysiological terms, in order to reach a wider scientific community. With this approach we address important questions like the feasibility of simulation of neural networks built using analog VLSI circuits.

2 The I&F circuit

The I&F neuron circuit is shown in Fig. 1. The circuit comprises a source follower M1-M2, used to control the spiking threshold voltage; an inverter with positive feedback M3-M7, for reducing the circuit’s power consumption; an inverter with controllable slew-rate M8-M11, for setting arbitrary refractory periods; a digital inverter M13-M14, for generating digital pulses; a current-mirror integrator M15-M19, for spike-frequency adaptation, and a minimum size transistor M20 for setting a leak current.

2.1 Circuit operation

The input current I_{inj} is integrated linearly by C_{mem} onto V_{mem} . The source-follower M1-M2, produces $V_{in} = \kappa(V_{mem} - V_{sf})$, where V_{sf} is a constant sub-threshold bias voltage and κ is the sub-threshold slope coefficient [12]. As V_{mem} increases and V_{in} approaches the threshold voltage of the first inverter, the feedback current I_{fb} starts to flow, increasing V_{mem} and V_{in} more rapidly. The positive feedback has the effect of making the inverter M3-M5 switch very rapidly, reducing dramatically its power dissipation.

A spike is emitted when V_{mem} is sufficiently high to make the first inverter switch, driving V_{spk} and V_{o2} to V_{dd} . During the spike emission period (for as long as V_{spk} is

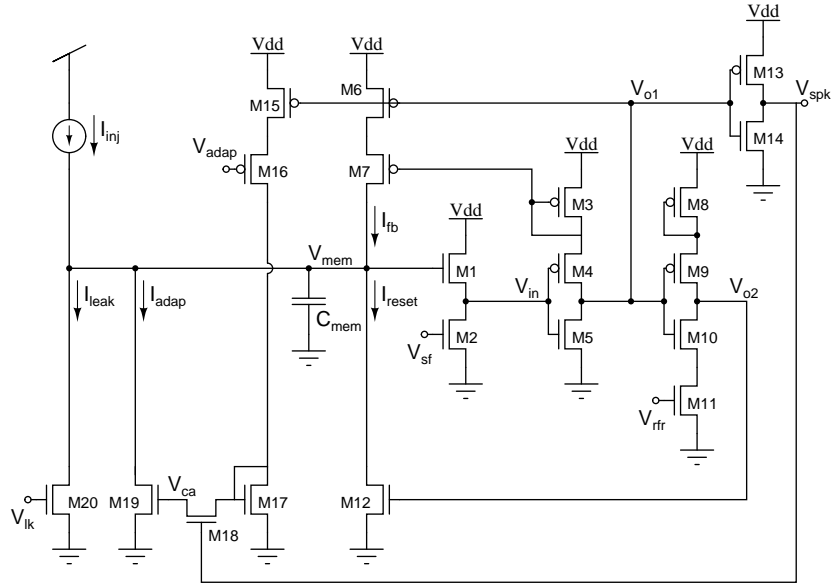


Fig. 1. Circuit diagram of the I&F neuron.

high), a current with amplitude set by V_{adap} is sourced into the gate-to-source parasitic capacitance of M19 on node V_{ca} . Thus, the voltage V_{ca} increases with every spike, and slowly leaks to zero through leakage currents when there is no spiking activity. As V_{ca} increases, a negative adaptation current I_{adap} exponentially proportional to V_{ca} is subtracted from the input, and the spiking frequency of the neuron is reduced over time.

Simultaneously, during the spike emission period, V_{o2} is high, the reset transistor M12 is fully open, and C_{mem} is discharged, bringing V_{mem} rapidly to Gnd . As V_{mem} (and V_{in}) go to ground, V_{o1} goes back to V_{dd} turning M10 fully on. The voltage V_{o2} is then discharged through the path M10-M11, at a rate set by V_{rfr} (and by the parasitic capacitance on node V_{o2}). As long as V_{o2} is sufficiently high, V_{mem} is clamped to ground. During this “refractory” period, the neuron cannot spike, as all the input current I_{inj} is absorbed by M12.

The adaptation mechanism implemented by the circuit is inspired by models of its neurophysiological counterpart [13, 14, 15]: the calcium concentration $[Ca^{2+}]$ is increased with every spike and decays exponentially to its resting value; if the dynamics of $[Ca^{2+}]$ is slow compared to the inter-spike intervals then the effective adaptation current is directly proportional to the spiking rate computed in some temporal window. This results had been extensively applied to investigate the steady state responses [16, 17] and the dynamic proprieties [17] of adapted neurons.

Figure 2(a) shows an action potential generated by injecting a constant current I_{inj} into the circuit and activating both spike-frequency adaptation and refractory period mechanisms. Figure 2(b) shows how different refractory period settings (V_{rfr}) saturate the maximum firing rate of the circuit at different levels.

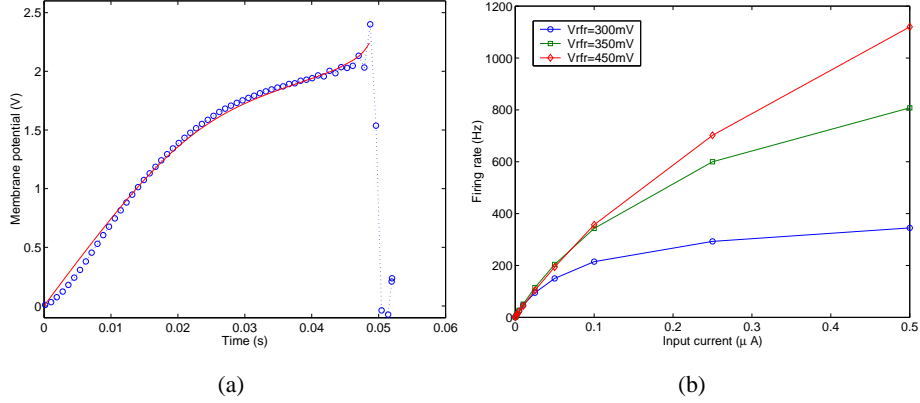


Fig. 2. (a) Measured data (circles) representing an action potential generated for a constant input current I_{inj} with spike-frequency adaptation and refractory period mechanisms activated. The data is fitted with the analytical model of eq. (5) (solid line). (b) Circuit's f - I curves (firing rate versus input current I_{inj}) for different refractory period settings.

2.2 Modeling the neuron's subthreshold behavior

The circuit presented does not implement a simple linear model of an I&F. Rather its positive feedback and spike-frequency adaptation mechanisms represent additional features that increase the model's complexity (and hopefully its computational capabilities). The overall current that the circuit receives is $I_{in} + I_{fb} - I_{adap}$, where I_{in} is the circuit's input current I_{inj} subtracted by the leak current I_{leak} (see Section 2.3), I_{fb} is the positive feedback current and I_{adap} is the adaptation current generated by the spike-frequency adaptation mechanism. We can use the transistor's weak-inversion equations [12] to compute the adaptation current:

$$I_{adap} = I_0 e^{\kappa \frac{V_{ca}}{U_T}} \quad (1)$$

where I_0 is the transistor's dark current [12] and U_T is the thermal voltage.

If we denote with C_a the parasitic gate-to-source capacitance on node V_{ca} of M19, and with C_p the parasitic gate-to-drain capacitance on M19, then:

$$V_{ca} = V_{ca_0} + \gamma V_{mem} \quad (2)$$

where $\gamma = \frac{C_p}{C_p + C_a}$ and V_{ca_0} is the steady-state voltage stored on C_a , updated with each spike.

To model the effect of the positive feedback we can assume, to first order approximation, that the current mirrored by M3, M7 is:

$$I_{fb} = I_1 e^{\kappa V_{in}} \quad (3)$$

where I_1 is a constant current flowing in the first inverter when both M4,M5 conduct, and $V_{in} = \kappa(V_{mem} - V_{sf})$ is the output of the source-follower M1,M2.

The equation modeling the subthreshold behavior of the neuron is:

$$C_0 \frac{d}{dt} V_{mem} = I_{in} + I_{fb} - I_{adap} \quad (4)$$

where $C_0 = C_m + \gamma C_a$. Substituting I_{adap} and I_{fb} with the equations derived above we obtain:

$$C_0 \frac{d}{dt} V_{mem} = I_{in} + \left[I_1 e^{-\kappa 2 \frac{V_{sf}}{U_T}} e^{\kappa 2 \frac{V_{mem}}{U_T}} \right] - \left[I_0 e^{\kappa \frac{V_{a0}}{U_T}} e^{\kappa \gamma \frac{V_{mem}}{U_T}} \left(1 - e^{-\frac{V_{mem}}{U_T}} \right) \right] \quad (5)$$

We fitted the experimental data by integrating eq. (5) numerically and using the parameters shown in Table 1 (see solid line of Fig. 2(a)). The initial part of the fit (for low values of V_{mem}) is not ideal because the equations used to model the source follower M1,M2 are correct only for values of V_{mem} sufficiently high.

$C_m = 0.66\text{pF}$	$I_{in} = 177\text{pA}$	$V_{sf} = 0.5\text{V}$
$C_a = 0.12\text{pF}$	$I_1 = 2.29\text{pA}$	$V_{a0} = 50\text{mV}$
$C_p = 500\text{fF}$	$I_0 = 100\text{fA}$	$\kappa = 0.6$

Table 1. Parameters used to fit the data of Fig. 2(a)

2.3 Stimulating the neuron circuit

To inject current into the neuron circuit we use an on-chip p-type transistor operating in the weak-inversion domain [12]. By changing the transistor's gate voltage we can generate the current:

$$I_{inj} = I_0 e^{\frac{\kappa}{U_T}(V_{dd}-V_p)} \quad (6)$$

where V_p is the p-type transistor's gate voltage that we can control. If we take into account the leak current I_{leak} sourced by the transistor M20 of Fig. 1 we can write the net input current to the circuit as:

$$I_{in} = I_{inj} - I_{leak} = I_0 e^{\frac{\kappa}{U_T}(V_{dd}-V_p)} - I_0 e^{\frac{\kappa}{U_T}V_{lk}} (1 - e^{-V_{mem}}) \quad (7)$$

We can write the *desired* input current that we want to use to stimulate the neuron as

$$I_{des} = I_{d0} \cdot \eta \quad (8)$$

where I_{d0} is a normalizing factor and η is a noisy signal with mean value μ and standard deviation (STD) σ .

We can force the net input current I_{in} to be the desired input current I_{des} if we break up the current source gate voltage V_p in the following way:

$$V_p = V_{p0} - \frac{U_T}{\kappa} \ln(C_0 + \eta) \quad (9)$$

with $\eta > -C_0$.

In this case the net input current becomes:

$$I_{in} = I_0 e^{\frac{\kappa}{U_T}(V_{dd}-V_{p0})} e^{\frac{\kappa}{U_T} \frac{U_T}{\kappa} \ln(C_0+\eta)} - I_{leak} \quad (10)$$

which becomes

$$I_{in} = I_p(C_0 + \eta) - I_{leak} \quad (11)$$

with

$$I_p = I_0 e^{\frac{\kappa}{U_T}(V_{dd}-V_{p0})} \quad (12)$$

If we set $I_{leak} = I_p C_0$ and $I_p = I_{d0}$ then $I_{in} = I_{des}$, and the signal η is directly proportional to the desired input current.

3 Results

We first tested the neuron with the adaptation mechanism turned off, injecting an input current with a given statistics, parameterized by mean and STD, and analyzing the output's statistics. Then we repeated the same tests with the adaptation turned on, analyzing the output's statistics also for variations of the adaptation strength.

3.1 General proprieties of the I&F circuit

We measured the I&F circuit's f - I curves for different values of the input current's variance and mean. The input current (I_{in}) is characterized by the statistical properties of η (see eq. (8)). The signal η is white noise with mean μ and STD σ . Figure 3 shows the f - I curves for different values of STD. All the curves were obtained by setting the refractory period to approximately 6.6 ms ($V_{r,fr} = 280$ mV).

The circuit's firing rate f has a dependence on the the refractory period (τ_r) of the type [18]:

$$f \approx \frac{1}{\tau_r + \frac{1}{I_{des}}} \quad (13)$$

Figure 2(b) shows f - I curves obtained for three different values of $V_{r,fr}$ (τ_r). The curves tend, in the limit of $\tau_r \rightarrow 0$, to a straight line with slope inversely proportional to the circuit's spiking threshold voltage, that can be modulated by the source-follower bias voltage V_{sf} (see Fig. 1).

We measured the distribution of the Inter-Spike Intervals (ISIs) generated by the circuit for three different values of τ_r , sweeping the mean input current. To analyze the statistic of these distributions, we measured their Coefficient of Variation (CV), given by the ratio between the ISI STD and its mean [19, 20]. Although the literature had

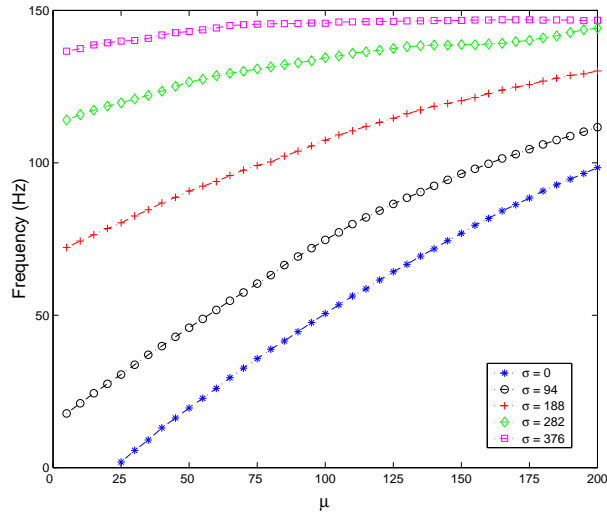


Fig. 3. f - I curves measured for five different values of σ .

extensively reported plots of CV against frequency or against ISI, we plotted the CV versus the mean input current to keep the notation consistent with the other figures presented here. The CVs reported for physiological-like values of τ_r (first two curves) are in accordance with theoretical [21] and experimental studies on neurons of layer 4 and 5 of the rat [16]. The ISI distribution for increasing input currents shifts toward lower mean-ISI, and its STD decreases. The refractory period constrains the distribution to remain above a certain ISI even if its STD decreases with the current. This is evident from the two traces with low value of $V_{r,fr}$ (high τ_r). Removing this constrain both mean and STD of the ISI can increase at the same rate and the resulting CV is approximately constant.

3.2 Effects of the adaptation on the I&F circuit

Next, we consider how the spike frequency adaptation mechanism influences the firing rate. We used six different values of V_{adap} (see Fig. 1). This voltage spanned values ranging from 4.10V to 4.35V with steps of 0.05V. We denoted these values respectively with very-high (VH), high (H) medium-high (MH), medium-low (ML), low (L), and very-low (VL) adaptation. In the following we will refer to this scale. All the collected data were obtained sweeping the mean input current by changing the mean value μ of the signal η (see eq. (8)).

Dynamic firing proprieties We measured the circuit's response to a series of depolarizing current steps with increasing values of μ and with $\sigma=0$. The neuron responds to current steps with frequencies that progressively adapt to lower steady state values (see Fig. 5). The circuit's adaptation current I_{adap} is integrated by a non-linear integrator (see M15-M19 of Fig. 1) and increases progressively with every spike (see also

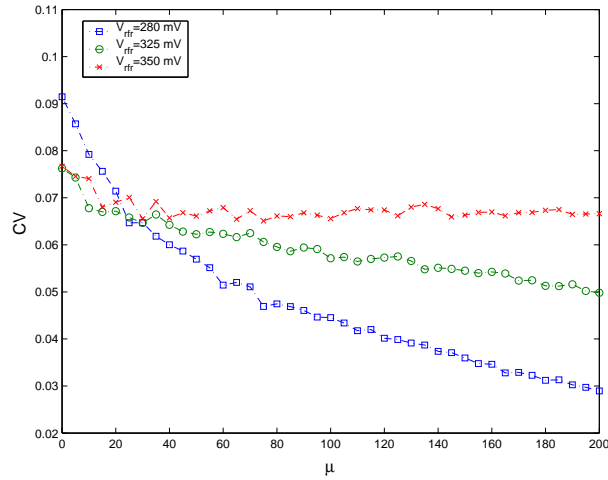


Fig. 4. Three different CVs for three values of V_{tr} (τ_r) plotted against μ of the input current with $\sigma=94$.

Section 2.2). As I_{adap} is subtracted from the input current I_{in} , the neuron's net input current progressively decreases, together with its output firing rate. In the steady state an equilibrium is reached when the adaptation current is balanced with the output firing rate (significantly lower than the initial one).

In Fig. 5 we show different instantaneous frequency response curves over time for increasing values of the input's step amplitude (μ) and for a fixed adaptation setting (VL). Initially, the instantaneous step response is directly proportional to the step's amplitude; however in the steady state regime, for increasing values of μ the mean firing rate first decreases and then monotonically increases. The same behavior was measured also changing adaptation values (see the inset in Fig. 8). During the transition to the steady state we can observe two behaviors:

short term transient - this transient is observed with any input step amplitude; the adaptation reaction time is inversely proportional to the injected current. Higher current injections require shorter periods to reduce the output firing rate. For input steps in the low current regime ($\mu \lesssim 50$), the circuit reaches the steady state right after this short-term transient. This adaptation mechanism has been reported in the literature with the name of *initial adaptation* [22]: it is observed when the neuron is injected with high enough currents, and it is modelled with a negative spike frequency dependent current.

long term transient - this transient is observed with step amplitudes greater than a certain threshold ($\mu \gtrsim 50$). The $f-t$ curves reach the steady state with an exponential decay time that decreases if the amplitude is increased. This adaptation mechanism has been reported in the literature with the name of *late adaptation* [23, 24, 25]: for strong enough input current the cell is unable to sustain the elevated activity imposed by the stimulation. After 2-3 seconds the mean spike frequency is constantly decaying.

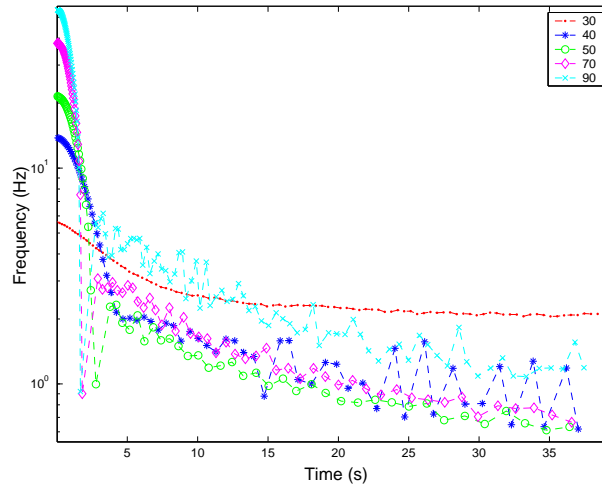


Fig. 5. Instantaneous frequency response of the circuit with adaptation value VL, for different values of the input step amplitude. Note the log-scale on the y-axis.

The exponential decay of the output firing rate observed for low input currents is consistent with our predictions. However, high input currents evoke second order and/or non-linear effects, as evident from the oscillations shown in Fig. 5.

In Fig. 6 we plotted different $f-t$ curves for different values of the adaptation settings and in Fig. 7 we plotted the variation of the frequency in the first time steps against the μ . Figure 6 shows how increasing levels of adaptation shorten the time required by the neuron to adapt and to reach a mean steady state value. From Fig. 7 we can deduce that in a restricted range of μ different adaptation settings produce approximately the same step response decay times.

Steady state firing proprieties In Fig. 8 we plotted different $f-I$ curves for different adaptation values. The curves in the inset show how increasing adaptation levels bring the steady state curves to be approximately linear at the rheobase, in agreement with theoretical [13] and experimental [16, 17] evidence. As expected, increasing adaptation values decrease the resulting firing rate f . High input currents clearly disrupt the adaptation mechanism: it has an abrupt loss of efficiency around a specific threshold of the incoming current for each adaptation level.

The variance of the net input current to a neuron embedded in a network increases with the number of connections it makes [19, 26, 27]. Hence we are interested in understanding how the effect of adaptation can change the $f-I$ curves for increasing levels of STD in the afferent current. In Fig. 8 we plotted different $f-I$ curves for different adaptation values. The figure is divided into four quadrants each referring to a different adaptation level. In each quadrant we plotted three curves for the three corresponding STD values. For medium and high adaptation values (ML, MH, H) the response of the neuron to inputs with high variance is still adapted. Note that the fluctuations (due to

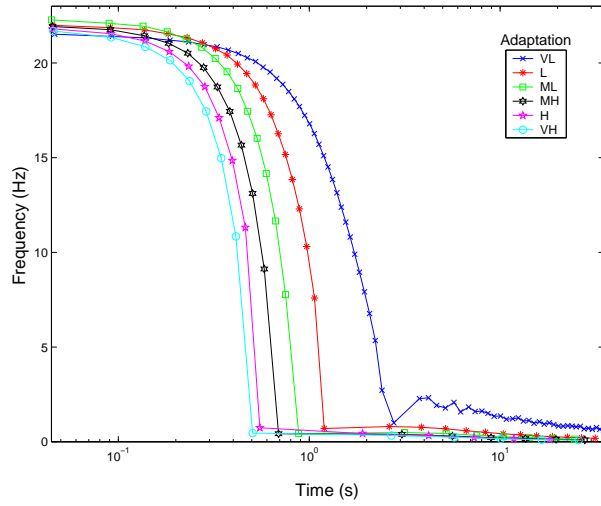


Fig. 6. Instantaneous frequency response for different adaptation values. The neuron adapts more quickly as the adaptation value increases. Note the log-scale on the x-axis.

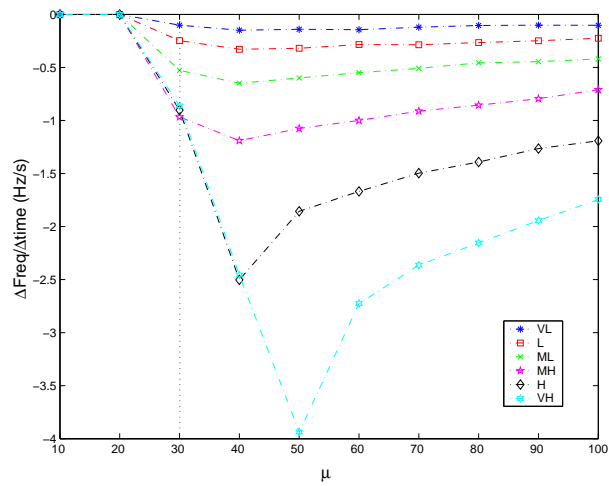


Fig. 7. Transient response slopes versus step amplitudes for different values of adaptation level. The thin dotted line at $\mu=30$ intersects the values computed from the data shown in Fig. 6

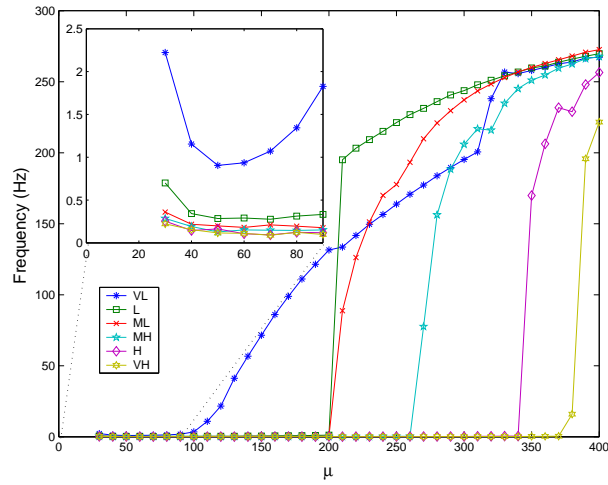


Fig. 8. f - I curves of the steady state response of the adapted neuron for various values of adaptation. The inset zooms the 0-90 range of μ .

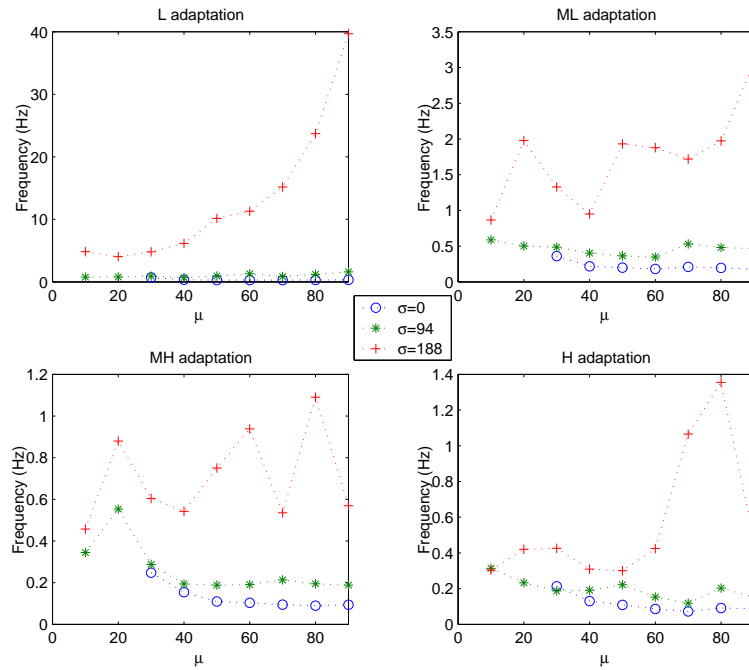


Fig. 9. f - I curves of the steady state response of the adapted neuron for various values of σ . The four quadrants show the plots for different values of the adaptation. Note the scales in each quadrant. Upper-left panel: frequency adaptation has less efficacy on the signal with high variance, even if the output firing rate is significantly lower to the non-adapted case (compare it to the third curve in Fig. 3). In all the other panels, the adaptation holds also for signals with high variance.

very small number of samples even if each test run for one minute) should be compared with the scale (i.e. the fluctuations are in the range of maximum 1Hz for the highest variance input).

4 Conclusions

We presented a novel analog VLSI circuit that implements a real-time model of a leaky I&F neuron. We characterized its response properties in a wide range of conditions, as a function of both the circuit's parameters and the statistics of the input signals. One of the most interesting properties of the circuit is its ability to model spike-frequency adaptation. We activated this feature, characterized the circuit, and showed how it exhibits different adapting behaviors when its operating conditions change. The inclusion of the adaptation mechanism addresses the question of which neurophysiological parameters in real neurons (spike induced Ca^{2+} influx, $[\text{Ca}^{2+}]$ decay time, ionic conductances) are actually captured by the VLSI circuit. Ahmed et al. [28] reported that spike frequency adaptation to a current step in neurons of the cat primary cortex can be well fitted by a single exponential curve depending on the degree of adaptation. This behavior is well captured by our circuit (see Fig. 5): the exponential rate decay is observed for low values of input currents, and the degree of adaptation can be set with V_{adap} . Moreover, the two behaviors (short and long term transients) in the dynamics (in Fig. 5) have been observed experimentally [22, 23, 24, 25]. The results presented here, together with the circuit's low-power characteristics [9] make it suitable for integration in very large arrays containing also synaptic circuits [2, 7, 29], and for the construction of massively parallel analog VLSI networks of spiking neurons.

Acknowledgements

This work was supported by the EU grant ALAVLSI (IST-2001-38099).

Bibliography

- [1] P., D., Abbott, L.F.: Theoretical Neuroscience. The MIT Press (2001)
- [2] Chicca, E., Indiveri, G., Douglas, R.: An adaptive silicon synapse. In: Proc. IEEE International Symposium on Circuits and Systems, IEEE (2003)
- [3] D'Andreagiovanni, M., Dante, V., Del Giudice, P., Mattia, M., Salina, G.: Emergent asynchronous, irregular firing in a deterministic analog VLSI recurrent network. In Rattay, F., ed.: Proceedings of the World Congress on Neuroinformatics. ARGESIM Reports, Vienna, ARGESIM/ASIM Verlag (2001) 468–77
- [4] Mead, C.: Analog VLSI and Neural Systems. Addison-Wesley, Reading, MA (1989)
- [5] Schultz, S.R., Jabri, M.A.: Analogue VLSI 'integrate-and-fire' neuron with frequency adaptation. *Electronic Letters* **31** (1995) 1357–1358
- [6] van Schaik, A.: Building blocks for electronic spiking neural networks. *Neural Networks* **14** (2001) 617–628
- [7] Boahen, K.: Communicating neuronal ensembles between neuromorphic chips. In Lande, T.S., ed.: *Neuromorphic Systems Engineering*. Kluwer Academic, Norwell, MA (1998) 229–259
- [8] Culurciello, E., Etienne-Cummings, R., Boahen, K.: Arbitrated address-event representation digital image sensor. *Electronics Letters* **37** (2001) 1443–1445
- [9] Indiveri, G.: A low-power adaptive integrate-and-fire neuron circuit. In: Proc. IEEE International Symposium on Circuits and Systems, IEEE (2003)
- [10] Mainen, Z., Sejnowski, T.: Reliability of spike timing in neocortical neurons. *Science* **268** (1995) 1503–1506
- [11] Destexhe, A., Rudolph, M., Fellous, J., Sejnowski, T.: Fluctuating synaptic conductances recreate in vivo-like activity in neocortical neurons. *Neuroscience* **107** (2001) 13–24
- [12] Liu, S.C., Kramer, J., Indiveri, G., Delbrück, T., Douglas, R.: Analog VLSI: Circuits and Principles. MIT Press (2002)
- [13] Ermentrout, B.: Linearization of F-I curves by adaptation. *Neural Comput.* **10** (1998) 1721–1729
- [14] Liu, Y., Wang, X.: Spike-Frequency Adaptation of a Generalized Leaky Integrate-and-Fire Model Neuron. *J. Comput. Neurosc.* **10** (2001) 25–45
- [15] Fuhrmann, G., Markram, H., Tsodyks, M.: Spike-Frequency Adaptation and neocortical rhythms. *J. Neurophysiology* **88** (2002) 761–770
- [16] Rauch, A., Camera, G.L., Luescher, H.R., Senn, W., Fusi, S.: Neocortical pyramidal cells respond as integrate-and-fire neurons to in vivo-like input currents. *J. Neurophysiol.* **79** (may 15, 2003)
- [17] Wang, X.: Calcium coding and adaptive temporal computation in cortical pyramidal neurons. *J. Neurophysiol.* **79** (1998) 1549–1566
- [18] Koch, C., Segev, I.: *Methods in Neural Modeling*. second edn. MIT Press (2001)
- [19] Tuckwell, H.: *Introduction to Theoretical Neurobiology*. Volume 2. Cambridge University Press, Cambridge, UK (1988)

- [20] Softky, W., Koch, C.: The highly irregular firing of cortical cells is inconsistent with temporal integration of random EPSPs. *J. Neurosci.* **13** (1993) 334–350
- [21] Fusi, S., Mattia, M.: Collective behaviour of networks with linear (VLSI) integrate-and-fire neurons. *Neural Computation* **11** (1999) 633–652
- [22] Schwindt, P., Crill, W.: Modification of current transmitted from apical dendrite to soma by blockade of voltage- and ca^{2+} -dependent conductances in rat neocortical pyramidal neurons. *J. Neurophysiol.* **78** (1997) 187–198
- [23] Schwindt, P., Spain, W., Crill, W.: Long-lasting reduction of excitability by a sodium-dependent potassium current in cat neocortical neurons. *J. Neurophysiol.* **61** (1989) 233–244
- [24] Sawczuk, A., Powers, R., Binder, M.: Contribution of outward currents to spike-frequency adaptation in hypoglossal motoneurons of the rat. *J. Neurophysiol.* **78** (1997) 2246–2253
- [25] Fleidervish, I., Friedman, A., Gutnick, M.: Slow inactivation of na^{+} current and slow cumulative spike adaptation in mouse and guinea-pig neocortical neurones in slices. *J. Physiol.* **493** (1996) 83–97
- [26] Amit, D., Tsodyks, M.: Quantitative study of attractor neural network retrieving at low spike rates. I. substrate-spikes, rates and neuronal gain. *Network: comput. in Neural Systems* **2** (1991) 259–274
- [27] Amit, D., Brunel, N.: Model of global spontaneous activity and local structured activity during delay periods in the cerebral cortex. *Cerebral Cortex* **7** (1997) 237–252
- [28] Ahmed, B., Anderson, J., Douglas, R., Martin, K., Whitteridge, D.: Estimates of the net excitatory currents evoked by visual stimulation of identified neurons in cat visual cortex. *Cereb. Cortex* **8** (1998) 462–476
- [29] Chicca, E., Badoni, D., Dante, V., D'Andreagiovanni, M., Salina, G., Carota, L., Fusi, S., Del Giudice, P.: A VLSI recurrent network of integrate-and-fire neurons connected by plastic synapses with long term memory. *IEEE Transactions on Neural Networks* **14** (2003) Special Issue on Hardware Implementation.